# A Bipolar Electrochemical Approach to Constructive Lithography: Metal/Monolayer Patterns via Consecutive Site-Defined Oxidation and Reduction

Assaf Zeira,[†] Jonathan Berson,[†] Isai Feldman,[‡] Rivka Maoz,*[,†] and Jacob Sagiv*[,†]

[†]Departments of Materials and Interfaces and [‡]Chemical Research Support, The Weizmann Institute of Science, Rehovot 76100, Israel

Ⓢ Supporting Information

ABSTRACT: Experimental evidence is presented, demonstrating the feasibility of a surface-patterning strategy that allows stepwise electrochemical generation and subsequent in situ metallization of patterns of carboxylic acid functions on the outer surfaces of highly ordered OTS monolayers assembled on silicon or on a flexible polymeric substrate. The patterning process can be implemented serially with scanning probes, which is shown to allow nanoscale patterning, or in a parallel stamping configuration here demonstrated on micrometric length scales with granular metal film stamps sandwiched between two monolayer-coated substrates. The metal film, consisting of silver deposited by evaporation through a patterned contact mask on the surface of one of the organic monolayers, functions as both a cathode in the printing of the monolayer patterns and an anodic source of metal in their subsequent metallization. An ultrathin water layer adsorbed on the metal grains by capillary condensation from a humid atmosphere plays the double role of electrolyte and a source of oxidizing species in the pattern printing process. It is shown that control over both the direction of pattern printing and metal transfer to one of the two monolayer surfaces can be accomplished by simple switching of the polarity of the applied voltage bias. Thus, the patterned metal film functions as a consumable "floating" stamp capable of two-way (forward−backward) electrochemical transfer of both information and matter between the contacting monolayer surfaces involved in the process. This rather unusual electrochemical behavior, resembling the electrochemical switching in nanoionic devices based on the transport of ions in solid ionic−electronic conductors, is derived from the nanoscale thickness of the water layer acting as an electrolyte and the bipolar (cathodic−anodic) nature of the water-coated metal grains in the metal film. The floating stamp concept introduced in this report paves the way to a series of unprecedented capabilities in surface patterning, which are particularly relevant to nanofabrication by chemical means and the engineering of a new class of molecular nanoionic systems.
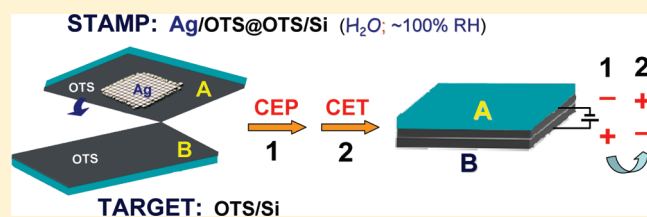
1. INTRODUCTION

Constructive lithography (CL) is a generic bottom-up fabrication strategy[1−4] based on the utilization of organic monolayers patterned by site-confined electrochemical processes that preserve their overall structural integrity as guiding templates in diverse post-patterning self-assembly processes.[1−20] In a typical implementation mode of the CL concept,[2,4] chemically active regions are generated within the otherwise inert outer surface of a self-assembled monolayer such as OTS/Si (monolayer on silicon derived from n-octadecyltrichlorosilane precursor molecules[21]) under conditions of virtual contact between the OTS/Si monolayer acting as a working electrode and a pattern-generation tool acting as the counter electrode. The pattern-generation tool may be a conductive SFM (scanning force microscope) tip that is programmed to serially inscribe patterns of modified surface functions on the top surface of a monolayer (constructive nanolithography, CNL)[2,6,22−24] or a conductive stamp that allows one-step parallel printing of similar but much larger surface patterns, covering micrometer-to-millimeter monolayer areas (constructive microlithography, CML).[4,12−15] Both the serial inscription and the parallel printing modes of pattern

generation exploit the same basic operation principle, the electrochemical modification of the monolayer being confined to those surface regions contacted by the biased tip or stamp.

Depending on the chemical constitution of the top monolayer surface and the polarity of the electrical bias applied, the pattern inscription/printing may involve either oxidation[2,15,23] or reduction[3,15] processes. To date, the local electrooxidation of the terminal −CH₃ groups (hydrophobic, chemically inert) of a highly ordered OTS/Si monolayer to −COOH functions (hydrophilic, chemically active) appears to offer by far the highest versatility in the implementation of the constructive lithography concept.[2,4−14,16−20,23] This is a consequence of the fact that OTS monolayers offer an unmatched combination of desirable properties. OTS is rather unique in that it is the lowest priced commercially available long-tail n-alkyl silane that can form high-quality self-assembled monolayers (in terms of molecular orientation, packing density, self-healing capability of

local structural defects, and chemical/structural robustness)[21] with chemically inert outer surfaces on a wide variety of different polar surfaces. The finding that the inert top surface of an OTS monolayer can be locally activated by a simple tip- or stamp-induced electrooxidation process[2,4] that preserves its highly ordered structure and the nonadherent lyophobic nature of the unmodified portions of its surface[19] paved the way to many different routes of surface chemical patterning and applications thereof.

In this electrooxidation process, the OTS/Si monolayer plays the role of anode and the SFM tip or the stamp plays the role of cathode, with the electrolyte being an ultrathin layer of water formed by capillary condensation from the ambient atmosphere within the contact area between the anode and the cathode. The interfacial water layer plays a key role both as an electrolyte and an electrochemical reagent by supplying, via electrolysis, the oxy species needed for the local conversion of methyl to carboxylic acid.[2,4,14] As far as the function of the interfacial water layer is concerned, the OTS patterning in constructive lithography is analogous to that of a semiconductor or a metal in local anodic oxidation lithography, whereby a surface pattern is inscribed or printed on the semiconductor or the metal surface with an electrically biased scanning tip[25−29] or metal stamp[29−33] operating in a humid atmosphere. The nondestructive electrooxidation of the outer OTS surface differs, however, from the anodic oxidation of a semiconductor or a metal surface in two fundamental aspects: (i) in the local anodic oxidation of a semiconductor or a metal, the patterning process depends on and is limited by charge and mass transport across the growing oxide layer produced in the process,[26] whereas in the monolayer case the oxidation is confined to just the outer atomic layer of the patterned surface facing the patterning tool;[2,4,6,14,23,29] (ii) the local anodic oxidation of a semiconductor or a metal creates a topographic difference of several nanometers between the modified and the unaffected surface regions, both of which are essentially hydrophilic,[25−33] whereas in the nondestructive electrooxidation of a monolayer such as OTS/Si the monolayer height is not significantly changed. The conversion of $-CH_3$ to $-COOH$ does, however, render the modified monolayer regions hydrophilic, as contrasted with the high hydrophobicity of the unaffected monolayer surface.[10,14,16,19] It follows from these differences that the monolayer system is exceptional in what concerns its compatibility with various postpatterning routes of bottom-up nanofabrication[2] as well as with some rather unusual pattern-generation configurations. Thus, the high wettability and reactivity contrasting the modified (hydrophilic, wettable, reactive) with the unmodified (hydrophobic, non wettable, inert) surface regions of nondestructively patterned OTS/Si monolayers are at the basis of their possible utilization as effective guiding templates in various self-assembly processes,[2,6,7,11−13,15−20] as in the advancement of the concept of contact electrochemical replication (CER) of hydrophilic−hydrophobic monolayer patterns.[14] In the latter process, the monolayer pattern itself is used as an electrochemical stamp, thus enabling the straightforward multiple replication of such patterns on other OTS/Si surfaces without the need to reuse a master stamp repeatedly in the printing of each replica.[14] Unlike conventional conductive stamps utilized in electrochemical patterning,[4,13,29−33] printable features in such flat monolayer stamps are not defined topographically but rather by their hydrophilicity as contrasted with the hydrophobicity of the surrounding monolayer surface, with the effective transfer of the pattern being facilitated by the selective

wetting-driven self-assembly[16,19] of a water-retaining hydrogel layer on the hydrophilic pattern sites.[14] Here and in additional forthcoming publications, we show how the high wettability and chemical reactivity contrast displayed by such hydrophilic−hydrophobic monolayer patterns may be usefully exploited in various other modes of contact electrochemical patterning.

In this article, we introduce a CL strategy, referred to as contact electrochemical patterning and transfer (CEP−CET), that allows consecutive printing (or inscription) and metallization of monolayer patterns via electrochemical processes carried out (in a humid atmosphere) either in a parallel contact configuration using a stamp or in a serial mode using a scanning probe that contacts selected sites on the monolayer surface. CEP−CET is shown to be applicable to OTS monolayers assembled on two different low-conductivity substrates—silicon and poly(vinyl alcohol) (PVA).[34]

The fabrication of metal-on-monolayer patterns by the present process differs in principle from both the adhesion-promoted transfer printing of a prefabricated metal film pattern from a metal-coated stamp to a more adherent target surface[35−38] and the various electrochemical metal-patterning processes involving bulk liquid electrolytes.[39−50] To our knowledge, the possible utilization of nondestructively patterned organic monolayers on nonmetallic solid substrates as stable templates for the electrochemical generation of planned metal-on-monolayer structures, rather than the common metal-on-metal deposition under a monolayer,[46,47,49] or in the monolayer-free regions of a metal surface coated with a patterned monolayer[45,47−49,51] or on a bare silicon surface,[52] is demonstrated here for the first time. This conceptually new approach offers a straightforward chemical route to the fabrication of robust monolayer-supported patterns of metal nanodots, conducting metal nanowires, and contact electrodes extending over the full range of lateral length scales from nanometer to millimeter, thus providing a unified methodology applicable to both the template-guided assembly of a new class of organic−inorganic nanodevices and their seamless electrical connection to the outside macroworld. Owing to the low conductivity of solid substrates compatible with the CEP−CET process, the electrical operation of such devices should be practically unaffected by the conductivity of the underlying substrate.[53]

Because the elucidation of the electrochemical processes effecting the observed surface transformations demands access to unequivocal tools of structural−chemical characterization, a major part of this article is devoted to a study of stamp-generated patterns with lateral dimensions in the range of tens of micrometers, which allowed a direct correlation of optical and SFM imaging with quantitative micro-FTIR (Fourier transform infrared) spectroscopic data collected from discrete, well-defined surface features. Examples of two different modes of consecutive pattern inscription and metallization with a scanning probe finally demonstrate the nanoscale applicability of the same monolayer patterning and pattern metallization principles while providing further insight into the electrochemical processes involved in the patterning and metal-transfer operations.

The experimental results reported here were obtained in a series of proof-of-concept experiments carried out for the purpose of establishing the feasibility of the CEP and CET operations and allow a basic understanding of the main characteristic features of this novel approach to surface patterning. It should therefore be noted that no systematic work has thus far been done in order to optimize the experimental procedures tried throughout this exploratory investigation.

2. METHODS AND MATERIALS

2.1. Fabrication of Stamp and Target Specimens. The OTS/ Si stamp and target specimens employed in the present CEP—CET experiments were ~10 mm ×15 mm silicon wafer substrates (Semiconductor Processing Co., Boston, double-side-polished, p-type, orientation ⟨100⟩, resistivity 8—11 Ω cm, 0.5 mm thick) coated on both sides with a highly ordered self-assembled OTS monolayer.[14,19,21] The backside OTS coating is needed in order to protect the unpatterned side of the stamp or the target from contamination that would interfere with the interpretation of the quantitative micro-FTIR spectra acquired in transmission through the silicon substrate.[14] Unpatterned carboxylic acid target surfaces (the CET experiment in Figure 5) were NTSox/ Si monolayers prepared by the in situ oxidation (with organic permanganate) of the terminal double-bond groups of self-assembled NTS/Si specimens[14] (monolayers derived from nonadecenyltrichlorosilane precursor molecules).[21] All procedures and materials employed in the assembly of the OTS and NTS monolayers and the conversion of NTS to NTSox were as described in ref 14. The quality control procedure applied routinely to each monolayer specimen prepared in this laboratory includes its characterization by quantitative FTIR spectroscopy,[14,21] SFM imaging,[6,14,19] and contact angle measurements,[19,21] to make sure beyond any doubt that only highly ordered, defect-free monolayers with uncontaminated outer surfaces are used in further studies.

Ag/OTS@OTS/Si stamp patterns were prepared by the e-beam evaporation of silver (Kurt J. Lesker, 99,999%) through contact masks consisting of TEM (transmission electron microscope) grids tightly pressed against the OTS/Si specimen in a specially built stainless steel holder that was also designed to prevent metal deposition on the unpatterned surface of the OTS/Si specimen. (Pattern notation Ag/OTS@OTS/Si is used to indicate silver-on-OTS features surrounded by bare OTS, to be distinguished from Ag/OTS/Si, a silver film covering the entire OTS surface.) Metal deposition was carried out in a homemade 6 kW e-beam evaporator equipped with a shutter that can control the passage of metal vapor to the sample. Samples were placed at a vertical distance of ~80 cm from the shutter, with the side on which metal is deposited away from it. Silver was deposited starting (for the first 5—10 nm) with an initial deposition rate of 0.05 nm/s and then continued at a rate of 0.25 nm/s. These careful conditions were employed to prevent any possible structural damage of the OTS monolayer on which the metal is deposited. That no such damage is caused to the monolayer and no migration of the metal through the monolayer to the underlying substrate occurs under these conditions were checked by removing the deposited metal film from the monolayer surface with adhesive tape or dissolving it in nitric acid or in an aqueous solution of iodine and potassium iodide (vide infra) and making sure that identical infrared spectra and contact angle data are recorded from same OTS/Si specimen before the deposition of the silver film and after its removal. Silver was also deposited under identical conditions on OTS monolayers assembled on fused silica slides, in which case the complete removal of the metal from the top surface of the undamaged monolayer could also be checked by UV—vis spectroscopy.

The PVA films in target specimens containing PVA (Figure 6) were prepared by casting a measured volume of a 4% aqueous solution of PVA (Mowiol 28-99, a fully hydrolyzed PVA material obtained from Kuraray, Germany) onto precleaned synthetic quartz (fused silica) slides or OTS/Si specimens and letting the water evaporate at ambient temperature in a dust-free atmosphere. Free-standing Ag-PVA stamp patterns were prepared by casting a measured volume of the aqueous PVA solution on an evaporated Ag/OTS/@OTS/Si stamp pattern (vide supra) followed by lift-off of the film left on the surface upon complete evaporation of the water in a dust-free atmosphere. The silver features in such stamps are almost completely embedded in the PVA film.

2.2. Electrochemical Stamping Experiments. The CEP—CET experiments (Figure 1) were performed similarly to the CER experiments reported in ref 14 using an electrical stamping device consisting of a humidity-controlled cell equipped with stainless steel holders for the stamp and the target specimens. The holders are electrically connected to a stabilized dc voltage generator, the output of which may be continuously varied over the range 3—80 V while also selecting the desired bias polarity. The upper holder (stamp) is mobile and may be pressed against the bottom holder (target) with variable mechanical force, manually or using calibrated weights. Equilibration with the humid atmosphere (at ~100% RH) was done for at least 20 min before bringing the stamp and target into contact.

Silver was quantitatively dissolved from patterned specimens (Figure 2) by immersion for ~30 min in HNO_3/H_2O (3% by vol) followed by prolonged overflow rinsing with pure water or by immersion for ~5 min in a solution of I_2 (1 g) and KI (4 g) in water (40 cm^3), followed by thorough rinsing with methanol and a final rinse with pure water.

2.3. SFM Patterning and Pattern Metallization Experiments: SFM and SEM Imaging. The serial CEP—CET experiments (Figures 7 and 8) were executed with an NTEGRA Aura SFM system (NT-MDT, Zelenograd, Russia) specially designed for various continuous and pulsed CNL modes of electrical nanopatterning and structural— electrical characterization of CNL-assembled surface architectures under controlled humidity at 55—60% RH. In the continuous two-run mode (Figure 8a), pattern inscription (first run) was done with W_2C-coated HSC20 contact probes (Team Nanotec GmbH, Villingen, Germany) and the metallization of inscribed features (second run) was done with NSC-36/Ti—Pt semicontact probes (MikroMasch, Tallinn, Estonia). The transfer of Ag to the tip and later from the tip to the surface was done in contact mode, and the imaging of metallized features was done in both contact and semicontact modes. All operations in the point-by-point one-run mode (Figure 8b) were executed with CSC-37/ Ti—Pt contact probes (MikroMasch) in contact mode. Higher-quality images of the resulting nanowires (Figure 8) were subsequently acquired with silver-free tips in semicontact mode. Silver was loaded onto the tip (Figure 7a) by scanning the surface of an evaporated silver film on OTS (Ag/OTS/Si) for 5 min with a bias of −10 V applied to the tip.

SFM images of the stamp-generated surface features (Figures 2, 3, 5, 6 and Figures S5 and S6 in the Supporting Information) were acquired as described before[6,14] with either an NTEGRA instrument (NT-MDT) offering DualScan mode[14] for wide-scan imaging up to 200 μm × 200 μm or with a SOLVER P47 instrument (NT-MDT) equipped with a 16 μm scanner[6,14] that was used for higher-resolution imaging in the range of several micrometers (Figures S1, S4, and S6 in the Supporting Information).

Scanning electron microscope (SEM) in-lens detector images (Figure S6A) were collected on an FEG LEO-Supra 55 VP instrument (Zeiss).

2.4. Micro-FTIR and X-ray Diffraction Measurements. The micro-FTIR spectra (Figure 3) were acquired as described before[14] on a Bruker Equinox 55 spectrometer connected to an IRscope II infrared microscope accessory equipped with a liquid-nitrogen-cooled MCT detector. The infrared microscope is also used as an optical microscope (equipped with a computer-connected digital camera) for optical imaging and the selection of sample regions from which IR spectra are to be recorded.

X-ray diffraction (XRD) spectra for the phase identification of silver (Figure S7) were obtained on a TTRAX III (Rigaku, Japan) theta—theta diffractometer equipped with a rotating Cu anode X-ray source operating at 50 kV and 200 mA and with a scintillation detector. The measurements were carried out in Bragg—Brentano mode ($2\theta/\theta$ scan). Six degrees offset is allowed to exclude the substrate peaks from the Si single crystal. The peak positions of the Bragg reflections and phase identification were determined using Jade 9 software (MDI).
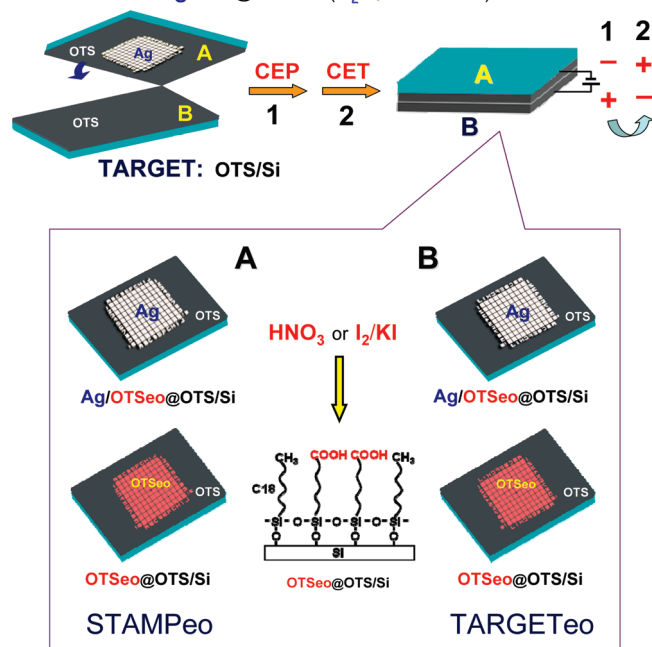
Figure 1. Schematic representation of the parallel CEP−CET process. (See the text.) The lower panel shows transferred and residual silver patterns on surface B (electrooxidized target—TARGETeo) and surface A (electrooxidized stamp—STAMPeo), respectively, and the corresponding monolayer prints (OTSeo@OTS/Si) revealed under the silver features upon removal of the metal from both surfaces with HNO$_3$ or I$_2$/KI.

3. RESULTS AND DISCUSSION

3.1. Parallel Contact Electrochemical Patterning and Transfer (CEP−CET) on Micrometric Length Scales. *3.1.1. Experimental Setup.* The basic stamping configuration employed in stepwise printing and in situ metallization of microscale monolayer patterns is depicted in Figure 1. In step 1 (CEP), a "STAMP" (A) consisting of a metal-on-monolayer pattern (Ag/OTS@OTS/Si) fabricated by evaporation through a TEM grid contact mask of a thin silver layer on a OTS/Si monolayer is pressed against a pristine OTS/Si "TARGET" monolayer (B) in a saturated humidity atmosphere (100% RH) while applying a voltage bias between A and B, with A being negative (cathode) and B being positive (anode).

As expected on the basis of a previously reported pattern printing process executed with plain metal grids or hydrogel/monolayer/silicon stamps,[4,14] a monolayer replica of the metal stamp features is indeed printed nondestructively in this manner on the target monolayer as a result of the local electrooxidation of the top −CH$_3$ groups of the target OTS to −COOH in those regions of the target touched by the wet features of the stamp.[54] The replica pattern printed on the target monolayer (OTSeo@OTS/Si) thus consists of OTSeo (electrooxidized OTS) regions corresponding to the metal features of the stamp, surrounded by the unmodified OTS monolayer background. In step 2 (CET), reversal of the bias polarity (with B now being the cathode and A being the anode) was found to result in the gradual transfer of the silver from A to B via an electrochemical process that involves

metal dissolution at A (anode), ionic transport across the nanoscale A−B gap, and metal redeposition on the OTSeo squares of B (cathode), resulting in a pattern of Ag/OTSeo features surrounded by the unmodified OTS monolayer (denoted as Ag/OTSeo@OTS/Si). To our initial surprise, it was further found that concomitantly with metal transfer the application of a sufficiently high voltage bias in step 2 effects the conversion of OTS to OTSeo also under the silver features of the STAMP monolayer itself. The OTSeo prints are revealed (as indicated in Figure 1, lower part) upon complete removal of the metal from both A and B by dissolution in nitric acid or in a solution of iodine and potassium iodide. Thus, the final product of the consecutive CEP (1) and CET (2) steps is the symmetric (mirror image) local electrooxidation of both the STAMP and TARGET monolayers (now denoted as STAMPeo and TARGETeo) according to the location of the silver features initially deposited on the STAMP and subsequently transferred to the TARGETeo.

As shown in the following text, these findings may be rationalized by considering the nanoscale confinement of the adsorbed water layer acting as an electrolyte and the bipolar electrochemical behavior[55−57] of the water-soaked granular metal film in the A/metal/B sandwich (Figure 1), which functions as a consumable "floating" stamp positioned between two OTS/Si monolayer specimens that may be equally patterned and metallized by it.

3.1.2. Evidence in Support of the Outcome of Steps 1 and 2 in Figure 1. To avoid ambiguities in the presentation and discussion of the experimental results, we retain in the following the nomenclature used in Figure 1, whereby the initial Ag/OTS@OTS/Si pattern produced by the evaporation of the metal on a OTS/Si monolayer is defined as STAMP and the pristine OTS/Si monolayer onto which the stamp pattern is to be printed is defined as TARGET. Consequently, TARGETeo and STAMPeo are the target and the stamp following the electrooxidative printing of the initial metal pattern on the respective OTS/Si monolayers, referred to as OTSeo@OTS/Si, and Ag/OTSeo@OTS/Si denotes transferred metal features on the OTSeo regions of the TARGETeo or residual metal features on the OTSeo regions of the STAMPeo (following the implementation of the CEP and CET operations). Thus, depending on the context, TARGETeo and STAMPeo may refer to either the respective metal-covered or metal-free OTSeo@OTS/Si patterns.

Figure 2 shows comparative optical micrographs and semi-contact-mode SFM images of an evaporated silver/monolayer micropattern (STAMP) produced with a TEM index grid as a contact mask and its mirror image replica (TARGETeo) resulting from the implementation (according to Figure 1) of the consecutive CEP (1) and CET (2) operations. Exampes of OTSeo features printed under the silver films and revealed upon removal of the metal from both the oxidized target and stamp surfaces are also shown. In this particular experiment, the metal was not completely transferred, as indicated by the somewhat lower measured heights of the replica metal features compared to those of the initial stamp pattern. The corrugation of the silver film is also seen to be higher in the replica pattern, which is, however, not a characteristic feature of the process. Depending on the experimental conditions, it is also possible to obtain transferred metal films that are considerably smoother and more compact than those of the initially prepared stamps (Supporting Information, Figures S1 and S5). The higher corrugation of the transferred silver film in Figure 2 may thus be a consequence of the incomplete transfer of the metal in this particular experiment.
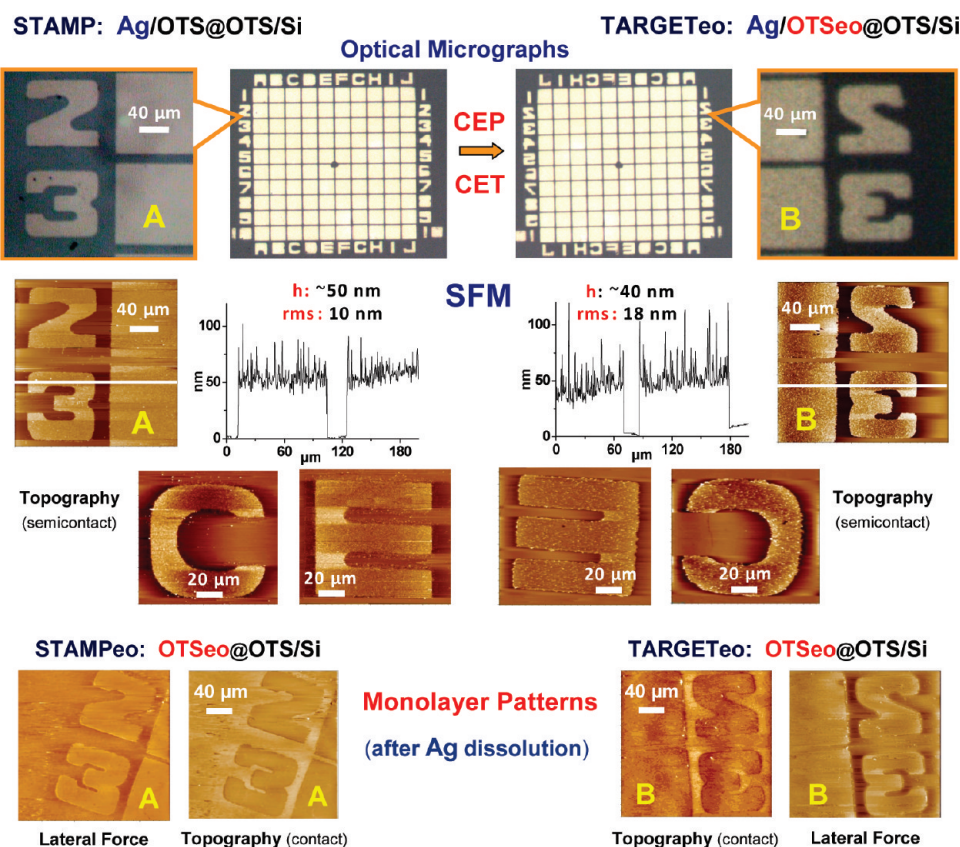
Figure 2. (Top) Comparative optical micrographs and SFM images obtained from identical selected regions of a silver/monolayer micropattern (STAMP: Ag/OTS@OTS/Si) and its mirror image replica (TARGETeo: Ag/OTSeo@OTS/Si) resulting from the implementation (according to Figure 1) of the consecutive CEP (1) and CET (2) operations. Height—width profiles taken from selected STAMP and corresponding TARGETeo regions are also shown for comparison. Heights (h) are given as average values, along with the respective rms values of the metal surface corrugation. (Bottom) Comparative SFM images taken from identical selected regions of the corresponding monolayer prints (OTSeo@OTS/Si) revealed upon removal of the transferred silver from the TARGETeo pattern and the residual silver from the STAMPeo pattern generated in the CET step (Methods and Materials). Squares A and B are the same as those in the corresponding A and B squares in the top images and in Figure 3. The STAMP pattern was fabricated using an SPI slim bar index grid (Ni 2290N, 200 mesh) as the contact mask (Methods and Materials). The CEP step was performed with a STAMP voltage bias of −40 V applied for 1 min, and the CET step was performed with +10 V applied for 10 min (Figure 1, Methods and Materials, and Figure S1 in the Supporting Information).

The presence of OTSeo prints under the silver features following the implementation of the CEP and CET steps can be qualitatively inferred from a simple scotch-tape test because the metal sticks well to printed monolayer areas while being easily removed by the adhesive tape from the initial STAMP (unmodified OTS) surface. Contact-mode SFM images taken from the OTSeo@OTS/Si monolayer patterns after complete dissolution of the transferred metal from TARGETeo and residual metal from STAMPeo (Figure 2, bottom) indeed demonstrate that both monolayer prints are faithful reproductions of the "floating" metal pattern. As expected on the basis of previous results obtained with nondestructively printed monolayer patterns of this kind,[4,14] here the printed OTSeo features also give rise to detectable contrast relative to the unmodified OTS surface in both the lateral force and corresponding topographic images, despite the lack of a significant real height difference between the OTSeo and OTS monolayers. The artifactual nature of such contact-mode topographic images was demonstrated in relation to both stamp-printed and tip-inscribed OTSeo@OTS/Si patterns,[4,6,14] with a thorough SFM study of this effect being reported in ref 23. This important aspect of the process is confirmed here by both the inversion of the

height contrast upon reversal of the scan direction[23] (Supporting Information, Figure S2) and the quantitative micro-FTIR spectra in Figure 3, which unequivocally demonstrate that the initial highly ordered structure of the OTS monolayer is fully preserved upon the electrooxidative conversion of its top methyls to carboxylic acid functions. Thus, the 2917 and 2949 cm^{-1} H—C—H stretching bands corresponding to the tail methylenes of OTS[21] and OTSeo[2,14] (fully extended all-trans conformation and perpendicular orientation of the hydrocarbon tails[21]) are superimposable whereas the disappearance of the 2957 cm^{-1} —CH$_3$ stretching band of OTS in the OTSeo spectra (bottom row curves) testifies to the quantitative conversion of the terminal —CH$_3$ groups of OTS to —COOH.[14]

3.1.3. Bipolar Electrochemical Mechanism of the CEP—CET Process. The overall experimental evidence obtained, including the results summarized in Figures 2 and 3 as well as that presented in the following text and in the Supporting Information (Figures S1, S5, and S6) convincingly points to the electrochemical nature of both the CEP and CET steps, ruling out a simple adhesion-promoted metal-transfer mechanism such as that reported in refs 35—38. Thus, no monolayer prints could be produced and no metal transfer was observed when the same
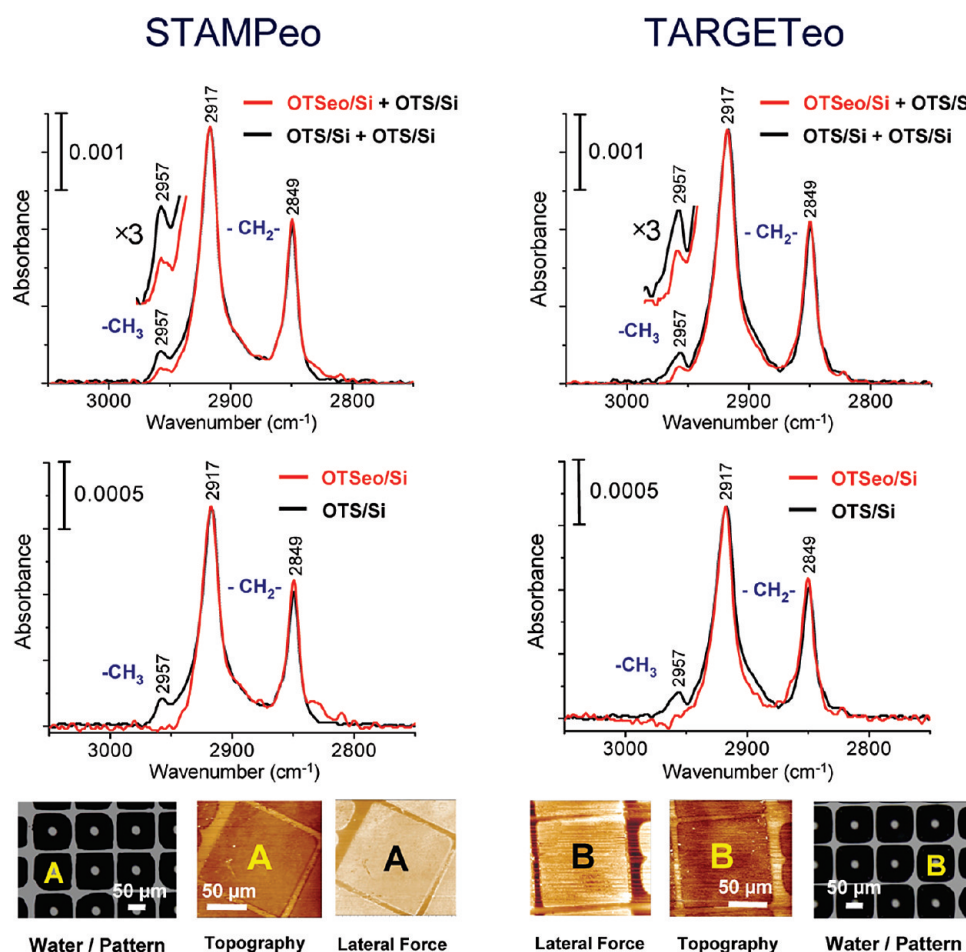
Figure 3. Quantitative micro-FTIR spectra (C—H stretching spectral region) acquired (with a 75 μm × 75 μm microscope aperture) from OTSeo/Si monolayer prints within square A of STAMPeo (left column) and square B of TARGETeo (right column) in the monolayer patterns displayed in Figure 2 (bottom) and from unaffected OTS/Si regions of the respective monolayer/silicon specimens. All displayed curves represent net spectral contributions of the respective organic monolayers, after mathematical subtraction of the spectral contributions of the corresponding bare silicon substrates. The notation OTSeo/Si + OTS/Si and OTS/Si + OTS/Si (in the top row curves) indicates the fact that, being recorded in transmission through double-side-polished silicon wafer substrates coated with an OTS monolayer also on their unmodified back sides, each of these spectral curves also contains the contribution of the respective back-side OTS/Si monolayer. The bottom-row curves show the corresponding net spectral contributions of each patterned front-side monolayer obtained by mathematical subtraction of the spectral contributions of the respective unmodified back-side monolayer (based on the fact that monolayer films assembled on each side of a double-side-polished wafer are identical). Spectra collected with an elongated rectangular aperture from hydrophobic bar regions separating the hydrophilic squares of the pattern (not shown) confirm that these consist of the unmodified OTS monolayer. Optical micrographs of water condensation patterns employed in the visualization of the monolayer patterns and the focusing of the FTIR microscope aperture on the desired surface sites[14] are shown below the respective spectral curves along with complete SFM images of squares A and B.

voltage bias sequences were applied to various monolayer—silver—monolayer sandwich configurations in the absence of environmental humidity, no transfer of metal from STAMP to TARGETeo could be realized without the reversal of the bias polarity, and considerable morphological differences have usually been observed between the evaporated metal features of a stamp pattern and their transferred metal replicas (Supporting Information, Figures S1, S5, and S6).

The appearance of an electrochemically generated monolayer print (OTSeo) of the metal pattern under the evaporated silver features of the stamp pattern (STAMPeo in Figure 2, bottom), in addition to the TARGETeo print, implies the presence of water at the metal—OTS interface in both TARGET and STAMP. This is possible because a granular silver film produced by evaporation is sufficiently hydrophilic to absorb water from the humid

ambient environment by capillary condensation within its entire intergrain volume. Water permeation into the metal film is controlled by its porosity, as demonstrated by the observation that all successful CEP—CET experiments reported here were performed with ~40-nm-thick silver film stamps that appear to be sufficiently porous, whereas the significantly poorer performance of ~80- and ~200-nm-thick silver film stamps correlates with their correspondingly smaller metal grain structure, higher compactness, and lower porosity (Supporting Information, Figures S3 and S4). Although the absorbed water most probably consists of an ultrathin coating of molecular-to-nanoscale thickness around each discrete metal grain and so occupies only a small fraction of the total film volume, the performance of a granular metal film of this type as an electrochemical pattern-transfer medium very much resembles that of the organic
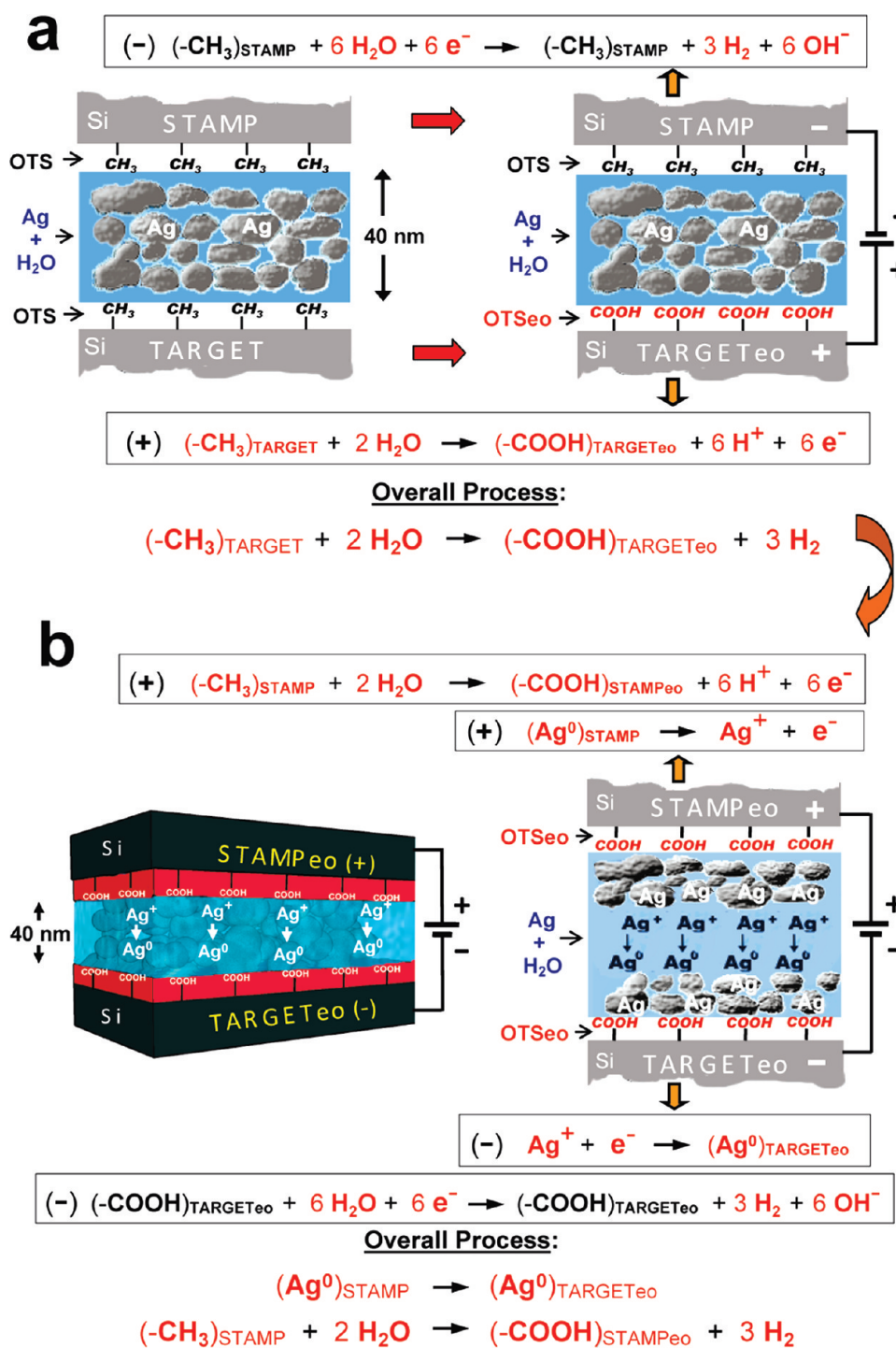
Figure 4. Schematic illustration of a water-soaked granular silver film sandwiched between two hydrophobic OTS/Si monolayers functioning as a "floating" stamp in the CEP−CET process. The relevant anodic and cathodic electrochemical reactions occurring at each monolayer−metal film interface are indicated (see the text): (a) Step 1 (CEP) in Figure 1 and (b) step 2 (CET) in Figure 1. The right-side scheme emphasizes the formation of a water gap that migrates from TARGETeo toward STAMPeo as the metal is transferred from STAMPeo to TARGETeo via electrochemical dissolution at STAMPeo, ion migration, and redeposition at TARGETeo (see the text), and the left-side scheme depicts in a somewhat more realistic fashion the hydrogel-like appearance of a water-soaked granular metal film that can confine and stabilize an ultrathin water layer between two highly hydrophobic surfaces.

hydrogel film used in the previously reported CER process.[14] However, unlike an organic hydrogel, a "metallic hydrogel" of this kind offers the double advantage that it can be deposited as a stable thin film on any surface, including hydrophobic surfaces

such as that of an OTS monolayer, and it can function as a supplier of both water and metal.

As depicted in Figure 4, when exposed to a humid atmosphere, the granular metal film can confine and stabilize an ultrathin layer

of water between two highly hydrophobic surfaces, which would be thermodynamically impossible in the absence of such a hydrophilic buffer interface. In the case of a laterally patterned metal film, the confined water layer enables the local (electrochemical) transfer of information and matter across the ~40 nm gap separating the two monolayer surfaces according to the geometry of the confining metal pattern (Figure 2). Metal transport between the two monolayer surfaces becomes possible owing to the bipolar character of the water-coated grains making up the metal film, which is a consequence of the large discrepancy between the high intragrain electronic conductivity and the much lower intergrain ionic conductivity within such a metal—water composite material.[55−57] When polarized in the high electric field produced upon the application of a bias voltage between the STAMP and TARGET monolayers, each discrete silver grain in the metal film would act as a dissolving anode on its side facing the cathodic monolayer and as a cathode on which metal is deposited on its side facing the anodic monolayer (Figure 4b).

The main Faradaic processes assumed to contribute to the CEP and CET steps, involving the STAMP and TARGET organic monolayers and the water-soaked silver film, are indicated in Figure 4a,b, respectively. In the pattern printing step (Figure 4a), the anodic (TARGET) reaction may conceivably involve, besides the oxidation of the −CH$_3$ groups of the OTS monolayer to −COOH, additional electrolysis of water with the evolution of oxygen, whereas the main cathodic (STAMP) reaction consists of regular water electrolysis with the evolution of hydrogen, which does not affect the OTS monolayer. In the metal-transfer step (Figure 4b), the roles of anode and cathode are reversed so that, upon the application of a sufficiently high voltage bias, the anodic reaction converting −CH$_3$ to −COOH now takes place at STAMP (which is thus converted to STAMPeo) and the cathodic reaction takes place at TARGETeo (i.e., the electrooxidized TARGET resulting from the initial pattern-printing step in Figure 4a). Concomitantly with the reactions taking place at the two monolayer—metal film interfaces, Ag$^+$ ions emanating from the anodic side of each metal grain within the silver film move toward the cathodic side of a grain located closer to the cathodic monolayer (TARGETeo) and deposit on it. In this manner, the electrochemical transfer of the metal from STAMPeo to TARGETeo is implemented via a "cascade" of metal dissolution—transport—deposition events taking place along the potential gradient between these two solid surfaces, the net result of which being that metal grains nucleating on the TARGETeo monolayer grow at the expense of dissolving metal grains closest to the STAMPeo monolayer. The oxidation of water and/or OH$^-$ ions generated at the TARGETeo monolayer surface (with the evolution of oxygen) and the reduction of water and/or H$^+$ ions generated at the STAMPeo monolayer surface (with the evolution of hydrogen) may also take place in the intergrain space in addition to the electrochemical silver dissolution and deposition. Equilibration with a humid atmosphere would ensure that water consumed in these processes is continuously replenished.

The generation of a STAMPeo monolayer print in step 2 of the CEP−CET process (as indicated in Figures 1 and 4b) implies that this step (CET) actually involves the CEP operation, now executed in a direction opposite to that of the step 1 CEP. However, one may note that if carried out below a certain bias voltage threshold, metal transfer in the CET step can be accomplished without electrooxidation of the STAMP monolayer. This was demonstrated in experiments carried out with bias voltages of 3 and 1 V. It was further found that, regardless of the bias voltage applied, silver could be transferred electrochemically only to functionalized monolayer surfaces receptive to the Ag$^+$ ion, such as carboxylic acid-rich surfaces that can bind silver ions via the formation of the silver carboxylate salt.[5] Successful metal transfer was thus achieved to either OTSeo surfaces in situ prepared in a preceding patterning step (as shown here) or ex situ prepared carboxylic acid[1,14,19] or thiol/disulfide functionalized monolayer surfaces[2,3,5] (vide infra), but not to unfunctionalized OTS targets. (See also CEP−CET nanoscale experiments in the following text.) This suggests that the nucleation and growth of silver grains on the cathodic monolayer is facilitated by a large local concentration of surface-immobilized Ag$^+$ ions. In the absence of appropriate Ag$^+$-binding monolayer functions, the metal will nucleate and deposit on preexisting metal grains located further away within the metal film, thus precluding the formation of intimate metal—organic monolayer contacts. These results further demonstrate that highly ordered silane monolayers such as those used here are impermeable to silver ions and atoms, with electrochemical metal deposition being exclusively confined to the top monolayer surface.

As we start with a configuration in which a silver film placed in intimate contact with the STAMP monolayer by virtue of its initial deposition on the STAMP is mechanically pressed against the TARGET (Figure 1), it is conceivable that, contrary to the symmetric distribution of interfacial water in the STAMP/TARGET space suggested in Figure 4a, the average gap between grains of the metal film and the TARGET monolayer should be larger than that at the STAMP monolayer. In the CET step, the gradual growth of metal grains in intimate contact with the carboxylic acid functions present on the TARGETeo surface implies that water initially adsorbed in the metal-TARGET gap must be squeezed out and forced to migrate gradually toward the STAMP or the newly formed STAMPeo surface (as depicted in Figure 4b, right-side scheme). Upon completion of the metal transfer, this water gap would reside at the metal−STAMPeo interface, with STAMPeo now being free of metal. Thus, the transfer of the metal from the stamp to target is coupled to the migration in the opposite direction of a thin water layer that defines the boundary between metal grains residing on each of the two surfaces involved in this process. Experimental support for the proposed asymmetry of the initial water distribution in the STAMP/TARGET space may be found in the asymmetry of the applied bias voltages needed for effective electrooxidation of the TARGET and STAMP monolayers (40 vs 10 V, respectively; see Figure 2 and Figure S1, Supporting Information).

Although this proposed scenario is consistent with the salient observed aspects of the CEP−CET process, the actual situation is expected to be more complex because metal grains separated from one another or from an organic monolayer surface by one or several-molecule-thick layers of water should also allow the passage of direct intergrain or grain—surface electronic current via electron tunneling/hopping mechanisms, in addition to the ionic currents associated with the Faradaic processes taking place at the metal—water and monolayer—water interfaces. The overall charge transmitted across the metal film is thus carried by an electronic current within each metal grain and by a combination of both ionic and electronic currents in the water-filled intergrain spaces. Because of the extremely small intergrain gaps, very large electric fields are expected in these regions upon the application of a voltage bias across the metal film, which should give rise to
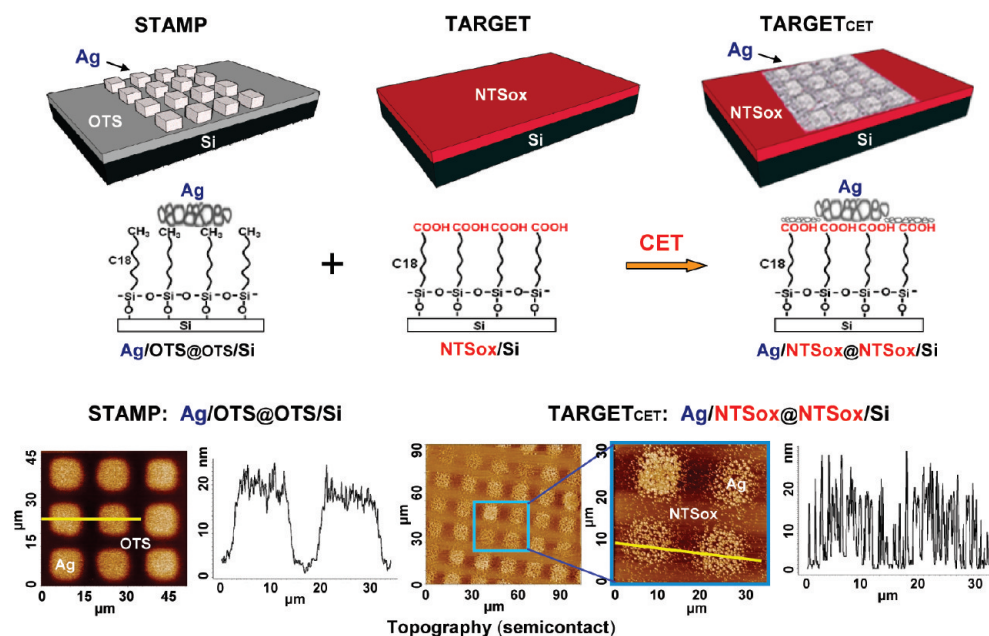
Figure 5. (Top) Scheme of contact electrochemical transfer of a silver/OTS pattern (STAMP; Ag/OTS@OTS/Si) to an unpatterned carboxylic acid-terminated monolayer surface (TARGET; NTSox/Si[1,14]) to create a pattern of Ag/NTSox features surrounded by the NTSox monolayer (TARGET$_{CET}$; Ag/NTSox@NTSox/Si). (Bottom) Examples of SFM images acquired from a STAMP and the corresponding TARGET$_{CET}$ patterns. The CET operation was performed with a voltage bias of +10 V applied to the STAMP for 10 min (Figure 1, Methods and Materials and Figure S1 in the Supporting Information).
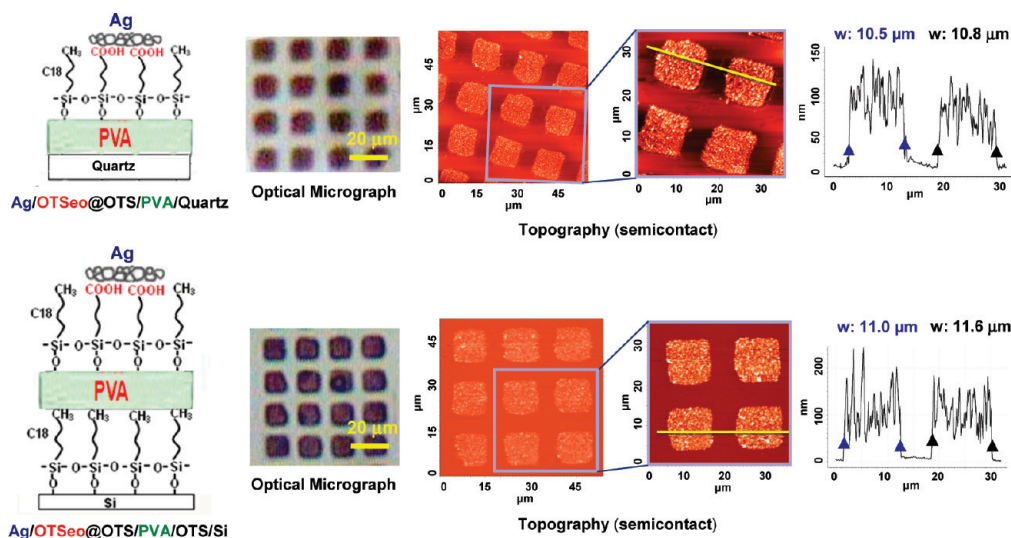

Figure 6. Examples of SFM images of transferred silver patterns produced by the CEP−CET process on targets consisting of (top row) a OTS monolayer assembled on a thick PVA film on quartz and (bottom row) a stratified composite film on silicon consisting of a OTS monolayer assembled on a thick PVA film produced on a OTS/Si monolayer (text and Methods and Materials).

unusually large ion migration currents and metal dissolution/deposition rates.[57]

Support of the proposed bipolar mechanism of metal dissolution−transport−deposition in the potential gradient established within a water-soaked granular metal film is further provided by the interesting observation of a self-correction effect that involves both vertical and lateral metal transport and so allows good replica patterns to be fabricated with less-perfect stamps (Supporting Information, Figures S5 and S6).

A final point of concern that has been addressed is the eventual formation of silver hydroxide/oxide via the ion combination and/or anodic oxidation reactions
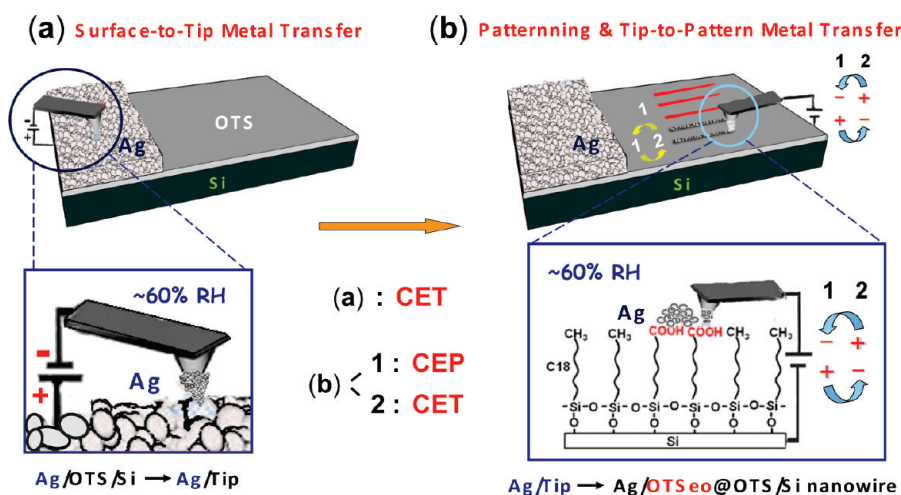
$$2Ag^+ + 2OH^- \rightarrow 2AgOH \rightarrow Ag_2O + H_2O$$

$$2Ag + 2OH^- \rightarrow Ag_2O + H_2O + 2e^-$$

Figure 7. Schematic representation of serial CEP−CET processes executed with scanning probes (text and Methods and Materials): (a) contact electrochemical transfer (CET) of silver from a silver film deposited on a OTS monolayer on silicon (Ag/OTS/Si) to a negatively biased SFM tip that scans the silver surface in contact mode and (b) the inscription of OTSeo lines on a OTS monolayer on silicon with a negatively biased tip (1, CEP), creating a nanopattern of OTSeo lines surrounded by the unaffected OTS monolayer background (OTSeo@OTS/Si). Silver is then deposited on selected OTSeo lines to create a pattern of Ag/OTSeo@OTS/Si nanowires by rewriting them with a silver-loaded tip to which a positive bias is applied (2, CET). The point-by-point inscription and metallization of OTSeo features are achieved using a silver-loaded tip to which a cyclic voltage bias is applied (1→2) so that OTS is first converted to OTSeo upon the application of a negative bias to the tip (1), followed by the transfer of silver from the tip to the surface upon reversal of the tip bias to a positive value (2).

which are, however, counterbalanced by possible cathodic and anodic decomposition via

$$Ag_2O + H_2O + 2e^- \rightarrow 2Ag + 2OH^-$$

and

$$2Ag_2O \rightarrow 4Ag^+ + O_2 + 4e^-$$
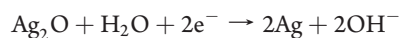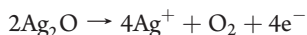
As demonstrated by X-ray diffraction data (Supporting Information, Figure S7), no silver oxide could be detected in silver films undergoing the present CEP−CET process.

3.1.4. Metal Pattern Transfer to a Hydrophilic Reactive Target Surface. As mentioned before, silver patterns can also be transferred electrochemically via the CET process to unpatterned monolayer surfaces receptive to Ag^+, such as ex situ-prepared carboxylic acid[1,14,19] or thiol-disulfide[2,3,5]-functionalized monolayer surfaces.[58] In this case, however, lateral spreading effects were found to preclude the faithful reproduction of the stamp pattern on the target surface.[58] An example of the lateral spreading of silver features transferred to a carboxylic acid surface is given in Figure 5, with similar results being obtained with thiol-disulfide target surfaces as well.[58] Compared with the Ag/OTSeo@OTS patterns in Figures 2 and S5 (Supporting Information), these results emphasize the importance of pattern conservation by the confinement of metal-binding sites (OTSeo) within a chemically inert monolayer background (OTS) that acts as an effective barrier against lateral spreading of the deposited metal features.

3.1.5. PVA: A Flexible Monolayer Substrate. Preliminary experimental results demonstrate the possible application of the CEP−CET methodology in the fabrication of stable metal/monolayer patterns on flexible polymeric films that may function as either or both target and stamp substrates. For example, the silver patterns in Figure 6 were produced on targets consisting of OTS monolayers assembled on thick, solution-cast PVA films[34] (∼0.1 mm thick) prepared on a synthetic quartz slide and on a silicon wafer substrate precoated with an OTS

monolayer, with the stamp patterns employed in these experiments being arrays of thin silver film squares embedded in a thick free-standing PVA film (Methods and Materials). The low conductivity of such PVA substrates, arising from their residual water and Na^+ ions content,[59] is thus sufficient for the successful implementation of the CEP−CET process. These results and particularly the possible access to complex stratified architectures such as the metal pattern/monolayer/PVA/monolayer/Si structure in Figure 6 suggest that CEP−CET might find interesting applications in the fabrication of novel flexible devices.

3.2. Serial CEP−CET on Nanometric Length Scales. Two implementation modes of the CEP−CET concept in a serial configuration, using a scanning probe instead of a stamp, are depicted in Figure 7. In both modes, silver metal is loaded onto a conductive SFM tip using a version of the CET process whereby the negatively biased tip is scanned over an evaporated Ag/OTS/Si film (Figure 7a) in a humidity-controlled atmosphere (at 55−60% RH). The metal is then transferred to selected active sites of an OTSeo@OTS/Si monolayer nanopattern inscribed with a negatively biased tip[2] (Figure 7b, operation 1, CEP) by rewriting them with the silver-loaded tip biased positively with respect to the monolayer surface (Figure 7b, operation 2, CET). The pattern inscription (CEP) may be done with the silver-loaded tip itself or with a different tip, followed by metallization of the inscribed sites of interest (CET) with the silver-loaded tip. If both operations are carried out with the silver-loaded tip, then one may choose either a "two-run" mode consisting of a continuous inscription of the pattern (first run) followed by the metallization of selected pattern sites (second run) inscribed in the first run or a "one-run" mode consisting of point-by-point pattern inscription and metallization. In the one-run mode, the bias applied to the tip is cycled between preset negative and positive voltage values at each point of the pattern that needs to be metallized (Figure 7b, operations 1 and 2, respectively).
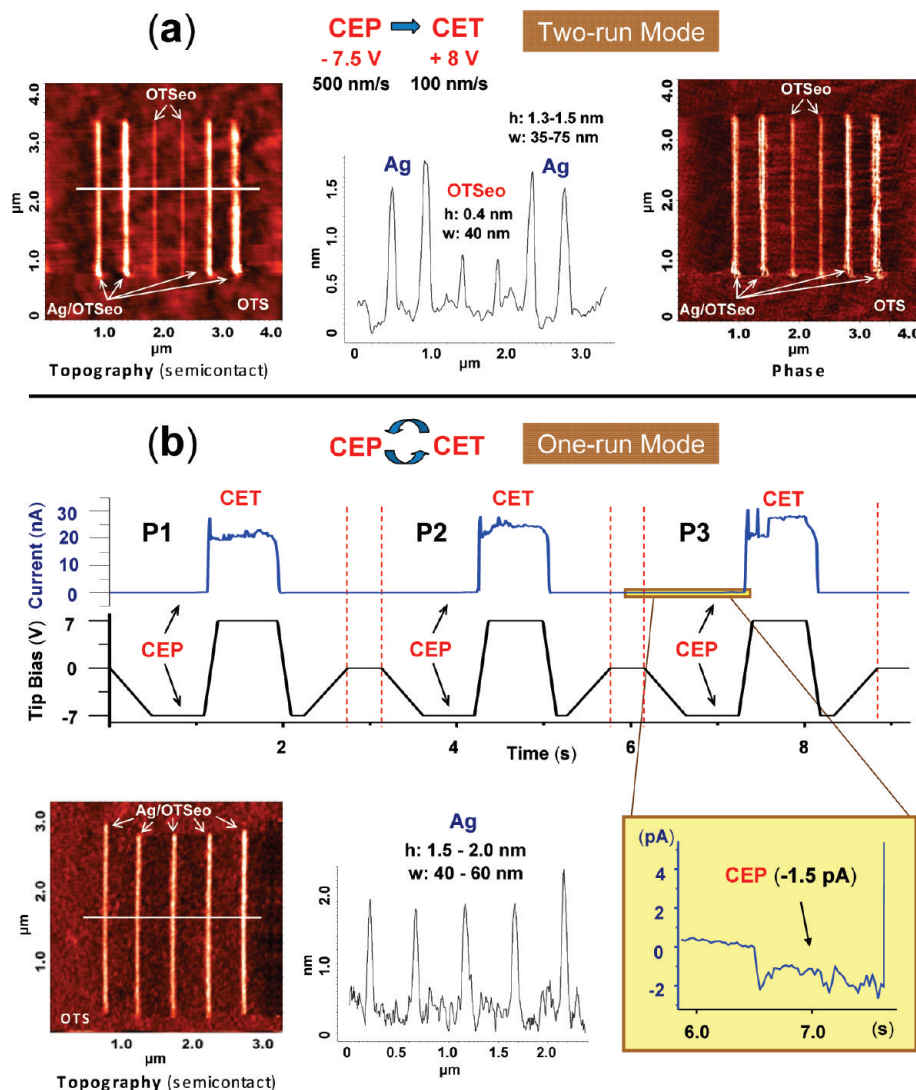
Figure 8. Experimental realization of serial CEP−CET processes according to the fabrication modes depicted in Figure 7 (text and Methods and Materials): (a) SFM images of nanowires fabricated in the continuous two-run mode showing four out of six OTSeo lines written with a negatively based silver-free tip (at −7.5 V and a speed of 500 nm/s in the vector mode of the SFM software) after being metallized by rewriting them with a positively biased silver-loaded tip (at +8 V and a speed of 100 nm/s) and (b) SFM data pertaining to silver nanowires fabricated in the point-by-point one-run mode with discrete points spaced 30 nm from one another. Currents flowing between the tip and surface were recorded while cycling the bias applied to the tip (using the spectroscopy mode of the SFM software) along the voltage path of 0 V → −7 V → +7 V → −7 V → 0 V (data are displayed for three consecutive points, P1, P2, P3, along one of the nanowires). CEP currents on the order of 1.5 pA (enlarged view of the CEP current region in P3) measured during the conversion of OTS to OTSeo are seen to jump to ∼20 nA during the transfer of the silver (CET) from the tip to the corresponding OTSeo dots. Capacitance-related current spikes are also visible. All CEP−CET experiments were performed at 55−60% RH in a humidity-controlled atmosphere.

Examples of the implementation of the two-run mode, using a silver-free tip for pattern inscription, and the one-run mode with a silver-loaded tip are given in Figure 8. In the continuous two-run mode (Figure 8a), silver wires with heights of 1.3−1.5 nm, generated on four out of the six inscribed OTSeo lines, are clearly identified in both the topographic and phase images.[60] In the point-by-point one-run mode (Figure 8b), the applied bias voltages and respective tip−surface currents were recorded during the inscription (CEP) and subsequent metallization (CET) of each dot along each of the five nanowires fabricated in this manner. The voltage−time versus current−time data obtained allow us to distinguish unequivocally between the CEP and CET steps because the currents recorded during the

electrochemical transfer of the silver (CET, ∼20 nA) are much larger than those recorded during the inscription of the corresponding OTSeo dots (CEP, ∼1.5 pA). Because in this mode the same tip is used to both inscribe and metallize each individual dot, the discrepancy between the respective CEP and CET currents cannot be attributed to spurious effects such as different conductivities of different tips or different tip−surface contact areas. The one-run mode thus offers a particularly valuable research tool because reliable comparative data of this kind may be difficult to obtain in stamping experiments where significant currents that do not contribute to the electrochemical transformations of interest can also flow between inactive regions of the stamp and the target.[14]

A number of control experiments confirm the validity of the correlation between the transfer of the metal from the tip to the surface and the high currents measured during the CET steps: using a silver-free tip and cycling the tip bias as in Figure 8b, currents on the order of 1 pA were measured in both the negative and positive voltage regions; using a silver-loaded tip to which only a positive bias cycle (0 V → + 7 V → 0 V) was applied, no OTSeo features were inscribed, no transfer of silver to the unmodified OTS surface was observed, and comparable low currents were measured; similar results were obtained using a silver-loaded tip and cycling the tip bias as in Figure 8b but in a dry atmosphere (∼4% RH). These experiments further demonstrate that under conditions of effective electrochemical metal transfer to carboxylic acid surface sites (OTSeo), silver is not deposited on the unfunctionalized OTS surface or under the monolayer, with the monolayer acting as an efficient barrier against the passage of silver ions and atoms.

With a separation of 30 nm between discrete inscribed dots and a measured lateral dot size of 40−60 nm, the point-by-point mode is seen to produce rather continuous metal nanowires (Figure 8b) that are apparently more uniform than those fabricated via the two-run mode, where the metal is continuously delivered to continuous OTSeo lines (Figure 8a). However, it should be noted that no optimization of experimental procedures has been attempted in any of these proof-of-concept experiments.

4. CONCLUDING REMARKS

The experimental evidence presented unequivocally demonstrates the electrochemical nature of both the monolayer pattern printing (CEP) and metal-to-monolayer transfer (CET) processes executed with thin film metal stamps floating in the nanometric gap between two contacting monolayers. CEP−CET represents an unprecedented approach to monolayer patterning and metallization, the main conceptual novelty of which is derived from the unusual experimental setup employed in the two-way (forward−backward) electrochemical transfer of both information and matter between the solid surfaces involved in the process.

With the macroscopic anode and cathode surfaces placed in virtual contact with one another (Figure 1), the CEP−CET experimental configuration cannot be rationalized without zooming in on the micro- and nanostructure of the system components. On the nanoscale (Figure 4), this electrochemical configuration is complex and uncommon not only because the metal grains of the stamp and the electrolyte (water) are intimately intermixed and occupy the same space region but even more so because of the huge disproportion between the total mass and volume of the metal grains and the liquid electrolyte coming in contact with them. The electrolyte is present in the form of an ultrathin, possibly molecular water layer separating the metal grains of the stamp electrode, which, from a macroscopic perspective, appears as a regular solid-phase material. Because of the large difference between the electronic conductivity of the metal and the ionic conductivity of the water, this rather peculiar metal−water composite material displays mixed electronic−ionic conductivity and bipolar (cathodic−anodic) character[55−57] of its metal grains. However, because only such ultrathin layers of water also separate the floating metal stamp from each of the organic monolayer electrodes, with water being laterally confined to the contact area between the metal

features of the stamp and the hydrophobic monolayer surfaces, mass transport within the entire monolayer−metal−monolayer interfacial space is expected to be governed by the rates of the Faradaic processes taking place at the various electrochemically active interfaces within the system rather than by diffusion in the electrolyte. This heterogeneous organic−inorganic nanosystem thus resembles the operation of nanoionic devices based on the transport of ions in solid ionic conductors,[61−66] which suggests attractive possibilities for the assembly of molecular nanoionic systems that would combine miniaturization and the flexibility of molecular design with the robustness of inorganic nanoionics.

The bipolar character of water-coated metal grains is presumably retained in the serial CEP−CET processes implemented with a scanning SFM tip, although in this case the tip−metal−monolayer configuration is not symmetrical as that in the parallel monolayer−metal−monolayer process implemented with a metal/monolayer stamp.

The consumable floating stamp concept demonstrated here with thin silver film stamps[67] offers a number of attractive novel capabilities, such as the straightforward creation of planned organic monolayer template patterns spanning lateral length scales from micrometer to centimeter and their nondestructive in situ metallization by the sacrificial consumption of the metal stamp itself, possible control of the final morphology of the resulting metal features, and the rare capability of self-correction (Supporting Information, Figures S5 and S6) in the fabrication of a replica of a less-perfect stamp pattern. Other unprecedented capabilities, offered by different versions of this approach that will be reported in future publications, are the parallel contact electrochemical metallization of monolayer patterns spanning all lateral length scales down to nanometer via the selective delivery of the metal from an unpatterned thin film metal stamp to the metal-binding sites of a prepatterned monolayer surface and the contact electrochemical replication[14] of such monolayer patterns using unpatterned metal or polymeric thin film floating stamps as pattern-transfer media. These capabilities pave the way to the multiple parallel replication of such monolayer and metallized monolayer patterns on all lateral length scales from nano to macro.

The fact that both the evaporated and transferred metal films reside on the outer monolayer surface and do not migrate through the monolayer to the underlying substrate is a necessary precondition for the successful implementation of the CEP−CET process. This is obviously a consequence of the compact structure and the exceptional structural robustness of highly ordered organosilane monolayers of the kind employed in this work, which withstand rather harsh chemical[21] and electrochemical conditions (Figures 2, 3, 5, 6, and 8). By comparison, patterned thiol/gold monolayers have usually been employed as electrochemical resists[46−49,51] rather than templates,[68] with metal deposition in such systems involving the establishment of direct contacts between the gold substrate and the deposited metal.[46−49,51] The nondestructive monolayer patterning and pattern metallization by the CEP−CET process is thus particularly valuable as a new and versatile synthetic capability for the advancement of a viable bottom-up fabrication methodology based on guided self-assembly on patterned monolayer templates,[19] including monolayers on polymeric substrates that could be used in the fabrication of flexible devices.

Unlike electrochemical patterning processes employing bulk liquid electrolytes,[39−50] in CEP−CET the electrolyte (interfacial adsorbed water) is carried by and strictly confined to the

electrochemically active areas of the stamp whereas both the target and the inactive areas of the stamp are highly hydrophobic and so not wetted by it. This unique CEP−CET feature imposes a strict localization of the electrochemical reactions and precludes the lateral spreading of the to-be-transferred information and material outside the target areas intentionally contacted by the active areas of the stamp. Moreover, the possible use of both hard stamp and hard target surfaces should render the CEP−CET approach free of the inherent limitations imposed by the deformability of soft polymeric stamps such as those usually employed in microcontact printing[69] and so further improve the fidelity of pattern reproduction. Some of the results obtained in the course of this study (Supporting Information, Figure S1) indeed suggest that nanometer resolution can be achieved. At this stage, however, a critical evaluation of the ultimate miniaturization and resolution attainable in the parallel CEP−CET process is limited by the size and quality of the evaporated metal film patterns employed as affordable stamp models in the present proof-of-concept study. These important issues as well as the elucidation of many other experimental details remain to be addressed in future work.

■ ASSOCIATED CONTENT

Ⓢ Supporting Information. Preliminary CEP−CET experiments: examining the effects of variable voltage bias and the length of time the voltage bias is applied in each step of the process. Topographic artifact in the contact mode imaging of OT-Seo@OTS/Si patterns. Photochemical assessment of the porous structure of the granular silver films employed as stamps in the present CEP−CET experiments. CET self-correction effect. X-ray diffraction data. This material is available free of charge via the Internet at http://pubs.acs.org.

■ AUTHOR INFORMATION

Corresponding Author
*E-mail: rivka.maoz@weizmann.ac.il; jacob.sagiv@weizmann.ac.il.

■ ACKNOWLEDGMENT

■ REFERENCES

(1) Maoz, R.; Cohen, S. R.; Sagiv, J. *Adv. Mater.* **1999**, *11*, 55–61.
(2) Maoz, R.; Frydman, E.; Cohen, S. R.; Sagiv, J. *Adv. Mater.* **2000**, *12*, 725–731.
(3) Maoz, R.; Frydman, E.; Cohen, S. R.; Sagiv, J. *Adv. Mater.* **2000**, *12*, 424–429.
(4) Hoeppener, S.; Maoz, R.; Sagiv, J. *Nano Lett.* **2003**, *3*, 761–767.
(5) Hoeppener, S.; Maoz, R.; Cohen, S. R.; Chi, L.; Fuchs, H.; Sagiv, J. *Adv. Mater.* **2002**, *14*, 1036–1041.
(6) Liu, S.; Maoz, R.; Sagiv, J. *Nano Lett.* **2004**, *4*, 845–851.
(7) Onclin, S.; Ravoo, B. J.; Reinhoudt, D. N. *Angew. Chem., Int. Ed.* **2005**, *44*, 6282–6304.
(8) Li, T.; Zhang, X.; Jiang, X.; Li, Y.; Du, Z. *Chin. Sci. Bull.* **2005**, *50*, 2560–2564.
(9) Cai, Y.; Ocko, B. M. *J. Am. Chem. Soc.* **2005**, *127*, 16287–16291.
(10) Checco, A.; Cai, Y. G.; Gang, O.; Ocko, B. M. *Ultramicroscopy* **2006**, *106*, 703–708.
(11) Hoeppener, S.; Susha, A. S.; Rogach, A. L.; Feldmann, J.; Schubert, U. S. *Curr. Nanosci.* **2006**, *2*, 135–141.
(12) Becer, C. R.; Haensch, C.; Hoeppener, S.; Schubert, U. S. *Small* **2007**, *3*, 220–225.
(13) Andruzzi, L.; Nickel, B.; Schwake, G.; Rädler, J. O.; Sohn, K. E.; Mates, T. E.; Kramer, E. J. *Surf. Sci.* **2007**, *601*, 4984–4992.
(14) Zeira, A.; Chowdhury, D.; Maoz, R.; Sagiv, J. *ACS Nano* **2008**, *2*, 2554–2568.
(15) Unruh, D. A.; Mauldin, C.; Pastine, S. J.; Rolandi, M.; Fréchet, J. M. J. *J. Am. Chem. Soc.* **2010**, *132*, 6890–6891.
(16) Chowdhury, D.; Maoz, R.; Sagiv, J. *Nano Lett.* **2007**, *7*, 1770–1778.
(17) Cai, Y. *Langmuir* **2008**, *24*, 337–343.
(18) Gao, P.; Cai, Y. *Ultramicroscopy* **2009**, *109*, 1023–1028.
(19) Zeira, A.; Chowdhury, D.; Hoeppener, S.; Liu, S.; Berson, J.; Cohen, S. R.; Maoz, R.; Sagiv, J. *Langmuir* **2009**, *25*, 13984–14001.
(20) Xu, J.; Park, S.; Wang, S.; Russell, T. P.; Ocko, B. M.; Checco, A. *Adv. Mater.* **2010**, *22*, 1–5.
(21) Wen, K.; Maoz, R.; Cohen, H.; Sagiv, J.; Gibaud, A.; Desert, A.; Ocko, B. M. *ACS Nano* **2008**, *2*, 579–599.
(22) Pignataro, B.; Licciardello, A.; Cataldo, S.; Marletta, G. *Mater. Sci. Eng., C* **2003**, *23*, 7–12.
(23) Wouters, D.; Willems, R.; Hoeppener, S.; Flipse, C. F. J.; Schubert, U. S. *Adv. Funct. Mater.* **2005**, *15*, 938–944.
(24) Yang, M.; Wouters, D.; Giesbers, M.; Schubert, U. S.; Zuilhof, H. *ACS Nano* **2009**, *3*, 2887–2900.
(25) Dagata, J. A. *Science* **1995**, *270*, 1625–1626 and references therein.
(26) Avouris, P.; Hertel, T.; Martel, R. *Appl. Phys. Lett.* **1997**, *71*, 285–287.
(27) García, R.; Calleja, M.; Rohrer, H. *J. Appl. Phys.* **1999**, *86*, 1898–1903.
(28) Gómez-Moñivas, S.; Sáenz, J. J.; Calleja, M.; García, R. *Phys. Rev. Lett.* **2003**, *91*, 056101(1−4).
(29) Simeone, F. C.; Albonetti, C.; Cavallini, M. *J. Phys. Chem. C* **2009**, *113*, 18987–18994.
(30) Cavallini, M.; Mei, P.; Biscarini, F.; García, R. *Appl. Phys. Lett.* **2003**, *83*, 5286–5288.
(31) Yokoo, A. *J. Vac. Sci. Technol., B* **2003**, *21*, 2966–2969.
(32) Farkas, N.; Comer, J. R.; Zhang, G.; Evans, E. A.; Ramsier, R. D.; Wight, S.; Dagata, J. A. *Appl. Phys. Lett.* **2004**, *85*, 5691–5693.
(33) Albonetti, C.; Martínez. J.; Losilla, N. S.; Greco, P.; Cavallini, M.; Borgatti, F.; Montecchi, M.; Pasquali, L.; García, R. Biscarini, F. *Nanotechnology* **2008**, *19*, 435303(1−9).
(34) Sagiv, J. *Isr. J. Chem.* **1979**, *18*, 339–345.
(35) Loo, Y.-L.; Willett, R. L.; Baldwin, K. W.; Rogers, J. A. *J. Am. Chem. Soc.* **2002**, *124*, 7654–7655.
(36) Menard, E.; Bilhaut, L.; Zaumseil, J.; Rogers, J. A. *Langmuir* **2004**, *20*, 6871–6878.
(37) Lee, B. H.; Cho, Y. H.; Lee, H.; Lee, K.−D.; Kim, S. H.; Sung, M. M. *Adv. Mater.* **2007**, *19*, 1714–1718.
(38) Strobel, S.; Harrer, S.; Blanco, G. P.; Scarpa, G.; Abstreiter, G.; Lugli, P.; Tornow, M. *Small* **2009**, *5*, 579–582.
(39) Schuster, R.; Kirchner, V.; Xia, X. H.; Bittner, A. M.; Ertl, G. *Phys. Rev. Lett.* **1998**, *80*, 5599–5602.
(40) Schuster, R.; Kirchner, V.; Allongue, P.; Ertl, G. *Science* **2000**, *289*, 98–101.
(41) Landolt, D.; Chauvy, P.-F.; Zinger, O. *Electrochim. Acta* **2003**, *48*, 3185–3201.
(42) Möller, P.; Fredenberg, M.; Dainese, M.; Aronsson, C.; Leisner, P.; Östling, M. *Microelectron. Eng.* **2006**, *83*, 1410–1413.

(43) Kolb, D. M.; Simeone, F. C. *Electrochim. Acta* **2005**, *50*, 2989–2996.

(44) Sheffer, M.; Mandler, D. *J. Electrochem. Soc.* **2008**, *155*, D203–D 208.

(45) Nelson, J. B.; Schwartz, D. T. *Langmuir* **2007**, *23*, 9661–9666.

(46) Felgenhauer, T.; Yan, C.; Geyer, W.; Rong, H.-T.; Gölzhäuser, A.; Buck, M. *Appl. Phys. Lett.* **2001**, *79*, 3323–3325.

(47) Pesika, N. S.; Fan, F.; Searson, P. C.; Stebe, K. J. *J. Am. Chem. Soc.* **2005**, *127*, 11960–11962.

(48) Seo, K.; Borguet, E. *Langmuir* **2006**, *22*, 1388–1391.

(49) Mullen, T. J.; Zhang, P.; Srinivasan, C.; Horn, M. W.; Weiss, P. S. *J. Electroanal. Chem.* **2008**, *621*, 229–237.

(50) Zhang, B.; Weng, Y.-Y.; Huang, X.-P.; Wang, M.; Peng, R.-W.; Ming, N.-B.; Yang, B.; Lu, N.; Chi, L. *Adv. Mater.* **2009**, *21*, 3576–3580.

(51) Zamborini, F. P.; Crooks, R. M. *J. Am. Chem. Soc.* **1998**, *120*, 9700–9701.

(52) Li, Y.; Maynor, W.; Liu, J. *J. Am. Chem. Soc.* **2001**, *123*, 2105–2106.

(53) Silver/monolayer features produced by the present approach were found to be electrically conductive. Their electrical characterization is in progress, and results of this work will be reported in due course.

(54) The TEM metal grids used by us as conductive stamps in the CML process produce monolayer replica prints corresponding to the grid bars.[4,14] Our initial incentive to the fabrication and use of the present metal/monolayer patterns as stamps originated in the desire to devise an affordable route to similar monolayer prints that are replicas of the isolated interbar spaces rather than the interconnected bars of a TEM grid.

(55) Plimley, R. E.; Wright, A. R. *Chem. Eng. Sci.* **1984**, *39*, 395–405.

(56) Bradley, J. C.; Chen, H.—M.; Crawford, J.; Eckert, J.; Ernazarova, K.; Kurzeja, T.; Lin, M.; McGee, M.; Nadler, W.; Stephens, S. G. *Nature* **1997**, *389*, 268–271.

(57) Bradley, J. C.; Dengra, S.; Gonzalez, G. A.; Marshall, G.; Molina, F. V. *J. Electroanal. Chem.* **1999**, *478*, 128–139.

(58) Zeira, A. Ph.D. Thesis, Weizmann Institute, May 2010.

(59) Sodium acetate is a byproduct of the manufacture of PVA by the alcoholysis of poly(vinyl acetate) with methanol using NaOH as a catalyst. Most of the sodium acetate is removed after alcoholysis from the final PVA product.

(60) In these semicontact images, the OTSeo lines display a small height of ca. 0.4 nm above the OTS background. In contact-mode images recorded after their inscription, the same OTSeo features appear with either small negative or positive height contrast relative to the OTS background, depending on the scan direction. As discussed before (Figure 2 and Figure S2, Supporting Information), this was shown to be an artifact caused by friction-topography "crosstalk" in the contact-mode imaging of heterogeneous surfaces with both hydrophilic (polar) and hydrophobic (nonpolar) regions.[4−6,14,19,23] A systematic study of the semicontact imaging of such tip-inscribed monolayer patterns remains to be performed.

(61) Kozicki, M. N.; Mitkova, M.; Park, M.; Balakrishnan, M.; Gopalan, C. *Superlattices Microstruct.* **2003**, *34*, 459–465.

(62) Lee, M.; O'Hayre, R.; Prinz, F. B.; Gür, T. M. *Appl. Phys. Lett.* **2004**, *85*, 3552–3554.

(63) Maier, J. *Nat. Mater.* **2005**, *4*, 805–815.

(64) Waser, R.; Aono, M. *Nat. Mater.* **2007**, *6*, 833–840.

(65) Terabe, K.; Hasegawa, T.; Liang, C.; Aono, M. *Adv. Mater.* **2007**, *8*, 536–542.

(66) Waser, R.; Dittmann, R.; Staikov, G.; Szot, K. *Adv. Mater.* **2009**, *21*, 2632–2663.

(67) Though not yet investigated, other metals should be applicable as well.

(68) A rare case of apparent electrochemical metal deposition on top of a functionalized thiol monolayer, which cannot, however, exclude the possibility of partial contact with the gold substrate via a defect-mediated deposition mechanism,[49] is reported in Baunach, T.; Ivanova, V.; Kolb, D. M.; Boyen, H.-G.; Ziemann, P.; Büttner, M.; Oelhafen, P. *Adv. Mater.* **2004**, *16*, 2024–2028.

(69) Sharpe, R. B. A.; Burdinski, D.; Huskens, J.; Zandvliet, H. J. W.; Reinhoudt, D. N.; Poelsema, B. *J. Am. Chem. Soc.* **2005**, *127*, 10344–10349.